Article

Structure

Structural Basis for VEGF-C Binding to Neuropilin-2 and Sequestration by a Soluble Splice Form

Graphical Abstract

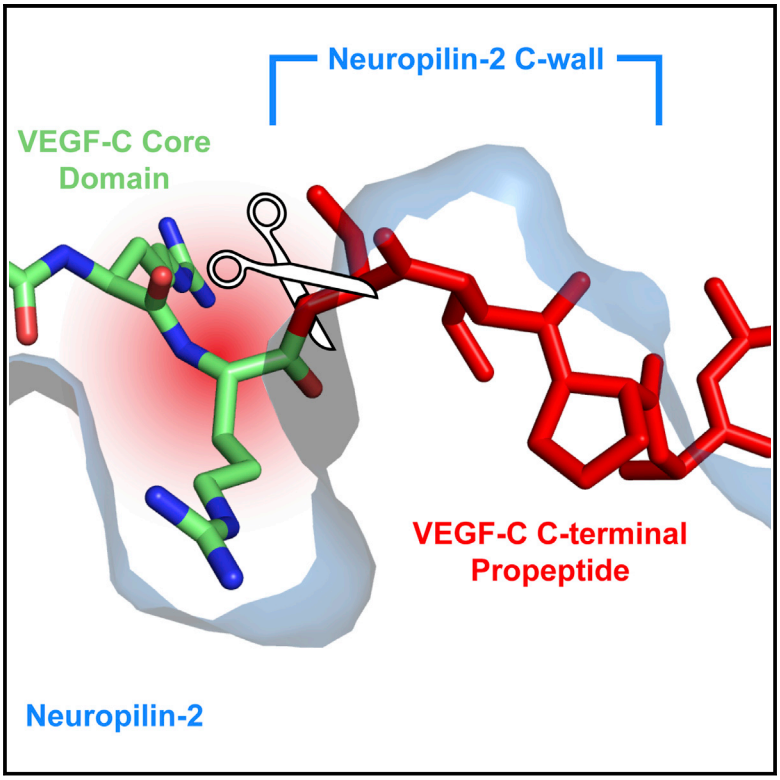

Authors

Matthew W. Parker,
Andrew D. Linkugel, ...,
Arthur M. Mercurio,
Craig W. Vander Kooi

Correspondence

craig.vanderkooi@uky.edu

In Brief

Vascular endothelial growth factor C (VEGF-C) is a potent lymphangiogenic cytokine that signals via the cell surface receptor Neuropilin-2 (Nrp2). Parker et al. demonstrate that VEGF-C binding to Nrp2 is regulated by C-terminal proteolytic maturation and identify a secreted splice form that functions as a selective inhibitor.

Highlights

- C-terminal processing of VEGF-C regulates direct binding to Nrp2
- Structure of the VEGF-C/Nrp2 complex demonstrates the basis for ligand binding
- Alternative Nrp2 splicing produces a soluble, dimeric receptor with novel structure
- Soluble Nrp2 functions as a potent antagonist of VEGF-C/Nrp2 binding

Accession Numbers

4QDQ
4QDR
4QDS

Parker et al., 2015, Structure *23*, 677–687
April 7, 2015
http://dx.doi.org/10.1016/j.str.2015.01.018

Structure
Article

Structural Basis for VEGF-C Binding to Neuropilin-2 and Sequestration by a Soluble Splice Form

Matthew W. Parker,[1] Andrew D. Linkugel,[1,2] Hira Lal Goel,[3] Tingting Wu,[1] Arthur M. Mercurio,[3] and Craig W. Vander Kooi[1,*]
[1]Department of Molecular and Cellular Biochemistry, Center for Structural Biology, University of Kentucky, Lexington, KY 40536, USA
[2]Washington University School of Medicine, St. Louis, MO 63110, USA
[3]Department of Molecular, Cell and Cancer Biology, University of Massachusetts Medical School, Worcester, MA 01605, USA
*Correspondence: craig.vanderkooi@uky.edu
http://dx.doi.org/10.1016/j.str.2015.01.018

SUMMARY

Vascular endothelial growth factor C (VEGF-C) is a potent lymphangiogenic cytokine that signals via the coordinated action of two cell surface receptors, Neuropilin-2 (Nrp2) and VEGFR-3. Diseases associated with both loss and gain of VEGF-C function, lymphedema and cancer, respectively, motivate studies of VEGF-C/Nrp2 binding and inhibition. Here, we demonstrate that VEGF-C binding to Nrp2 is regulated by C-terminal proteolytic maturation. The structure of the VEGF-C C terminus in complex with the ligand binding domains of Nrp2 demonstrates that a cryptic Nrp2 binding motif is released upon proteolysis, allowing specific engagement with the b1 domain of Nrp2. Based on the identified structural requirements for Nrp2 binding to VEGF-C, we hypothesized that the endogenous secreted splice form of Nrp2, s_9Nrp2, may function as a selective inhibitor of VEGF-C. We find that s_9Nrp2 forms a stable dimer that potently inhibits VEGF-C/Nrp2 binding and cellular signaling. These data provide critical insight into VEGF-C/Nrp2 binding and inhibition.

INTRODUCTION

The vascular endothelial growth factor (VEGF) family of cytokines are critical regulators of endothelial cell function. There are five VEGF family members: VEGF-A, -B, -C, -D, and placental growth factor (PlGF). Of these five, VEGF-C and VEGF-D selectively control lymphangiogenesis. While they show partially overlapping biological activity and physical properties, VEGF-C is essential for viability, whereas VEGF-D is not (Baldwin et al., 2005; Karkkainen et al., 2004). Endothelial cells of homozygous VEGF-C knockout mice do not sprout to form lymphatic vessels, which results in an alymphatic embryo and embryonic lethality (Karkkainen et al., 2004). Overexpression of VEGF-C results in selective induction of lymphatic but not vascular endothelial cell proliferation and lymphatic vessel enlargement (Jeltsch et al., 1997). In addition to its critical physiological role, VEGF-C signaling is also important for pathological lymphangiogenesis, which is associated with both aberrant loss of function in lymphedema (Saaristo et al., 2002) and gain of function in tumorigenesis and metastasis (Caunt et al., 2008; Ellis, 2006; Stacker et al., 2002).

VEGF-C signals via the coordinated activity of two families of endothelial cell surface receptors, the VEGF receptor (VEGFR) family of receptor tyrosine kinases (RTK) (reviewed in Stuttfeld and Ballmer-Hofer, 2009) and the Neuropilin (Nrp) family of coreceptors (reviewed in Parker et al., 2012a). VEGF-C function is specifically mediated through VEGFR-2/3 (Joukov et al., 1996; Kukk et al., 1996; Lymboussaki et al., 1999) and Nrp2 (Karkkainen et al., 2001; Xu et al., 2010), with VEGF-C capable of simultaneously engaging both families of receptors (Favier et al., 2006). VEGFR-2/3 have dual functionality in both angiogenesis and lymphangiogenesis (reviewed in Lohela et al., 2009). In contrast, Nrp2 knockout mice display normal angiogenesis but abnormal lymphatic vessel development (Yuan et al., 2002), similar to the tissue-specific function observed in the VEGF-C knockout (Karkkainen et al., 2004). Intriguingly, it has also been demonstrated that Nrp2 can function in VEGF-C signaling independent of its role as a coreceptor for VEGFR (Caunt et al., 2008).

Each member of the VEGF family of ligands is produced in multiple forms by either alternative splicing (e.g., VEGF-A, -B, and PlGF) or proteolytic processing (e.g., VEGF-C and -D) (Holmes and Zachary, 2005). In all cases, an invariant core cystine-knot domain, which specifically interacts with VEGFR, is combined with a variable C-terminal domain. VEGF-C is synthesized as a proprotein with N- and C-terminal domains flanking the central core cystine-knot domain. Prior to secretion, the C-terminal propeptide is cleaved followed by extracellular cleavage of the N terminus (Joukov et al., 1997). These processing events critically alter both the physiological and pathological bioactivity of VEGF-C (Siegfried et al., 2003). The mature dual-processed VEGF-C shows dramatically enhanced stimulatory activity in situ (McColl et al., 2003) and loss of C-terminal processing ablates function in vivo (Khatib et al., 2010). However, the physical basis for the enhanced activity of the mature form of VEGF-C remains unclear and has been connected to different properties, including differential receptor binding and interactions with heparin/extracellular matrix (ECM) (Harris et al., 2013; Joukov et al., 1997; Karpanen et al., 2006). The role of VEGF-C proteolytic maturation in regulating Nrp2 binding is unknown.

The structural basis for VEGF-C binding to VEGFR-2/3 has recently been elucidated and was shown to involve the invariant cystine-knot domain of VEGF-C binding to the N-terminal

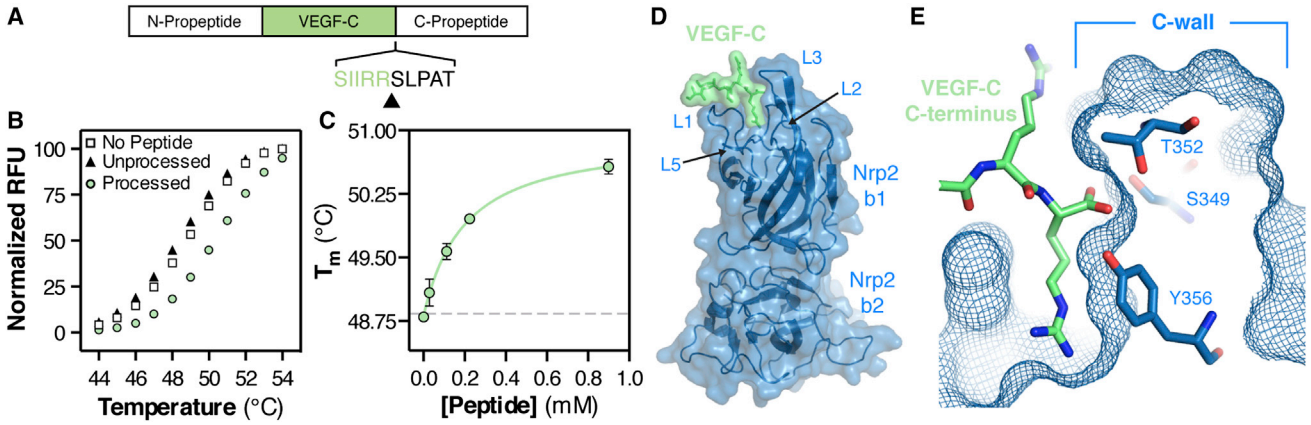

Figure 1. Crystal Structure of the VEGF-C/Nrp2 Complex Reveals the Basis for Proteolytic-Dependent Binding

(A) Organization of the VEGF-C proprotein and site of C-terminal processing (black arrow).

(B) Peptides corresponding to processed (green circle) and unprocessed (black triangle) VEGF-C were assayed for the ability to bind Nrp2-b1b2 as measured by DSF thermal shift assay. Peptides were added to Nrp2-b1b2 to a final concentration of 0.5 mM and melting was monitored between 20°C and 90°C. All samples were measured in triplicate, and a representative melting curve is shown for each. RFU, relative fluorescence units.

(C) Processed VEGF-C dose-dependently enhances the Nrp2-b1b2 T_m. Error bars indicate the SD of the three measurements.

(D) Structure of Nrp2-b1b2 (blue) in complex with the C terminus of VEGF-C (green).

(E) Cross-section of the Nrp2 binding pocket demonstrates that the free carboxy terminus of VEGF-C is buried against the Nrp2 C-wall, which is formed by the third coagulation factor loop.

domains of VEGFR-2 and VEGFR-3 (Leppanen et al., 2010, 2013). However, the structural basis for VEGF-C binding to Nrp2 remains to be determined. Alternative splicing and proteolysis modify the C-terminal variable region of VEGF and regulate Nrp binding (Makinen et al., 1999; Parker et al., 2012c; Soker et al., 1998). It has been demonstrated that Nrp1 binds the C-terminal basic domain of the Semaphorin-3 (Sema3) and VEGF family of ligands (He and Tessier-Lavigne, 1997; Soker et al., 1996), utilizing a binding pocket for ligands that contain a C-terminal arginine (Parker et al., 2010, 2012c; Vander Kooi et al., 2007; von Wronski et al., 2006). Importantly, the Sema3 family of ligands undergo furin-dependent proteolytic maturation within their C-terminal domain, a process that liberates an extended basic sequence and directly regulates bioactivity and Nrp binding (Adams et al., 1997; Parker et al., 2010, 2013).

Nrp2-dependent VEGF-C signaling is important in a variety of tumors and overexpression of these factors is correlated with advanced-stage disease and poor prognosis (Ellis, 2006; Stacker et al., 2002). Thus, specific Nrp2/VEGF-C inhibitors are of clinical interest. Soluble receptor fragments are common endogenous inhibitors (Albuquerque et al., 2009; Ambati et al., 2006; Kendall and Thomas, 1993; Rose-John and Heinrich, 1994). A soluble Nrp1 isoform was first identified as an endogenous inhibitor of prostate cancer in vivo (Gagnon et al., 2000). Soluble extracellular domain fragments can also be engineered for use clinically, including VEGF-trap (Aflibercept), a chimeric VEGFR-1/2-Fc fusion, which is an inhibitor of VEGF-A (Holash et al., 2002). A soluble splice form of Nrp2, s_9Nrp2, has been identified at the transcript level (Rossignol et al., 2000). s_9Nrp2 is produced by intron inclusion, which contains an in-frame stop codon. This stop codon is located prior to the transmembrane domain and is thus predicted to produce a secreted form of Nrp2. Interestingly, the insertion occurs in the middle of the second coagulation factor domain (b2), rather than in an interdomain region. The two Nrp2 coagulation factor domains (b1b2) form an integral unit (Appleton et al., 2007), and thus, the nature of the production and function of s_9Nrp2 is unclear. Further, domains b1b2 of Nrp2 have been demonstrated to bind VEGF-C (Karpanen et al., 2006), bringing into question whether this soluble splice form contains the structural requirements necessary to bind and sequester its ligands.

Here, we demonstrate that removal of the VEGF-C C-terminal propeptide directly regulates binding to Nrp2. The structure of the mature VEGF-C C terminus in complex with Nrp2 demonstrates that a cryptic Nrp2-binding motif is liberated upon C-terminal processing. This offers the first structural insight into the physical basis for VEGF-C binding to Nrp2, showing that the proteolytically liberated C-terminal arginine of VEGF-C directly binds the Nrp2 b1 domain. Mutagenesis of both VEGF-C and Nrp2 confirms the critical nature of the VEGF-C C-terminal sequence in Nrp2-b1 binding. Understanding the physical interactions underlying VEGF-C/Nrp2 binding led us to consider mechanisms for VEGF-C inhibition. The secreted Nrp2 splice form, s_9Nrp2, contains an intact Nrp2 b1 domain but a subsequent stop codon, and we assessed its function as a pathway-specific inhibitor. Strikingly, this soluble receptor forms a disulfide-linked dimer with two tightly integrated b1 domains and functions as a potent inhibitor of VEGF-C binding to Nrp2.

RESULTS

Structural Basis for Proteolytic-Dependent VEGF-C Binding to Nrp2

VEGF-C is synthesized as a proprotein with N- and C-terminal propeptides. Removal of the VEGF-C C-terminal propeptide critically regulates its bioactivity. C-terminal processing of VEGF-C liberates a polypeptide stretch rich in basic amino acids that terminates with a diarginine sequence (Figure 1A), a structural motif

Table 1. Data Collection and Refinement Statistics

Construct	Nrp2-VEGF-C	Nrp2-T319R	s_9Nrp2^B
Data Collection			
Beamline	APS 22-ID	APS 22-BM	APS 22-ID
Wavelength	1.0000	1.0000	1.0000
Space group	$P2_1$	$P2_12_12_1$	$P2_12_12$
Cell dimensions (Å)	41.05, 120.81, 69.84	34.90, 70.76, 122.97	69.36, 91.39, 67.33
Cell dimensions (°)	90.0, 103.29, 90.0	90.0, 90.0, 90.0	90.0, 90.0, 90.0
Unique reflections	44,081	12,223	16,303
Completeness (%)	90.6 (82.0)	96.4 (83.2)	94.1 (79.8)
Resolution (Å)	1.95 (2.02–1.95)	2.40 (2.49–2.40)	2.40 (2.49–2.40)
R_{merge} (%)	9.9 (46.6)	8.0 (29.2)	9.9 (32.7)
Redundancy	5.1 (4.2)	6.8 (5.9)	4.4 (4.1)
$I/\sigma(I)$	13.1 (3.0)	29.4 (5.1)	12.3 (3.2)
Refinement			
Resolution limits (Å)	20.00 (1.95)	20.00 (2.40)	20.00 (2.40)
No. reflections/no. to compute R_{free}	41,511/2,140	11,490/586	15,439/821
$R(R_{free})$	21.0 (24.1)	20.1 (25.5)	21.0 (26.4)
No. protein residues	632	313	361
No. solvent/ion molecules	333	123	107
Root-mean-square deviation bond (Å)	0.006	0.008	0.006
Root-mean-square deviation angle (°)	1.11	1.19	1.04
Protein Geometry			
Ramachandran outlier/favored (%)	0/96.7	0/96.1	0/96.7
Residues with bad bonds/angles	0/0	0/0	0/0
Rotamer outliers	0	0	0

conserved across the VEGF and Sema3 family of ligands and known to be important for Nrp1 binding. Thus, we hypothesized that processing of VEGF-C may directly regulate a physical interaction with Nrp2. To test this hypothesis, we produced peptides corresponding to the unprocessed (215-RQVHSIIRRSLPA-227) and processed (215-RQVHSIIRR-223) VEGF-C C terminus and measured the ability of each peptide to bind Nrp2 domains b1b2 using a differential scanning fluorimetry (DSF) thermal shift assay (Figure 1B). Processed VEGF-C significantly stabilized Nrp2-b1b2 (T_m 48.8°C ± 0.06°C to 50.3°C ± 0.05°C), while unprocessed VEGF-C showed no effect (T_m 48.4°C ± 0.04°C). Further, the processed VEGF-C peptide showed dose-dependent saturable binding to Nrp2-b1b2 with an apparent dissociation constant K_D = 199 μM ± 71 μM (Figure 1C). These data demonstrate that C-terminal proteolytic maturation directly regulates VEGF-C binding to Nrp2.

To define the physical basis for proteolytic-dependent binding of VEGF-C to Nrp2, we determined the crystal structure of the processed VEGF-C C terminus in complex with Nrp2 domains b1b2. The C-terminal five amino acids of mature VEGF-C (219-SIIRR-223), which are strictly conserved across species and also with VEGF-D, were fused to the C terminus of human Nrp2 domains b1b2 (residues 276–595). The fusion protein was expressed in *Escherichia coli*, purified, and crystallized. The structure was solved by molecular replacement and was refined to a resolution of 1.9 Å (Figure 1D; Table 1). There were two molecules in the asymmetric unit oriented in an antiparallel fashion (Figure S1A). Both molecules demonstrated specific binding of the VEGF-C encoded residues via an intermolecular interaction with a symmetry-related molecule.

Analysis of the structure reveals that VEGF-C (green) engages a binding pocket formed by the Nrp2-b1 (blue) coagulation factor loops (Figures 1D, S1B, and S1C). Indeed, this interloop cleft uniquely accommodates the C-terminal residue of processed VEGF-C (Figure 1E). The free carboxy terminus of VEGF-C is integrated into the binding pocket through interactions with residues from the third coagulation factor loop (L3) of Nrp2-b1, which form a wall at one side of the binding pocket (C-wall). Specifically, an extensive hydrogen bond network forms between the VEGF-C-free C-terminal carboxylate and the side chains of the C-wall residues S349, T352, and Y356 (Figure 1E). Importantly, the position of the C-wall would preclude binding of the unprocessed protein, providing a physical mechanism for the observed proteolytic-dependent binding of VEGF-C to Nrp2-b1b2.

Characterization of the VEGF-C/Nrp2 Interaction

Clear electron density for the VEGF-C-encoded region was observed, permitting modeling of both the VEGF-C polypeptide and interfacing solvent that bridge the two molecules (Figure 2A). Analysis of the VEGF-C/Nrp2 interface reveals direct interactions between VEGF-C and residues within the L1, L5, and L3 loops of Nrp2-b1 (Figure 2B), the regions that show the largest conformational changes when comparing the bound structure with the

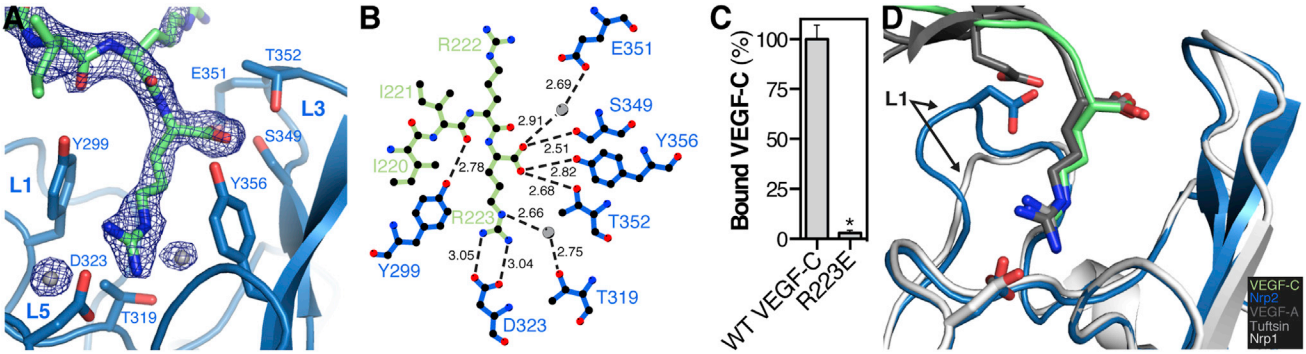

Figure 2. Mechanism of VEGF-C Binding to Nrp2

(A) Zoom of the intermolecular interface between Nrp2 (blue) and VEGF-C (green) with the $2F_o - F_c$ electron density map for VEGF-C contoured at 1.0σ. Interfacing water is shown as gray spheres.

(B) Ligplot+ generated representation of the interaction between VEGF-C (green) and Nrp2 (blue). Bond distances (Å) are labeled in black, and water is shown as gray spheres.

(C) Nrp2 binding was compared between VEGF-C and VEGF-C R223E. Binding was measured in triplicate and is reported as mean ± SD (*$p < 0.05$). WT, wild-type.

(D) Superimposition of the VEGF-A HBD/Nrp1 complex (PDB 4DEQ) and the tuftsin/Nrp1 complex (PDB 2ORZ) onto the structure of the VEGF-C/Nrp2 complex demonstrates the shared and unique modes of engagement within this ligand/receptor family.

previously reported apo structure (Figure S2) (Appleton et al., 2007). In addition to the hydrogen bond network formed between the VEGF-C free carboxy terminus and the Nrp2 L3 loop, the side chain of the VEGF-C C-terminal arginine, R223, forms extensive interactions with the Nrp2 binding pocket. The guanidinium of VEGF-C R223 forms a salt bridge with the Nrp2-b1 L5 loop residue D323. In addition, the aliphatic portion of the R223 side chain displays extensive van der Waals interactions with two tyrosine residues of Nrp2-b1 that demarcate the sides of the binding pocket, Y299 (L1 loop) and Y356 (L3 loop). In addition to interactions mediated by VEGF-C R223, there is a hydrogen bond between the backbone carbonyl of I221 and the aromatic hydroxyl of Nrp2 Y299.

While protein-protein binding is primarily mediated by direct interactions between polypeptide chains, interfacing solvent also plays a critical role in stabilizing protein-protein complexes (Janin, 1999; Karplus and Faerman, 1994). Three water molecules, two of which bridge the interaction between VEGF-C and Nrp2, are observed in the binding site. One solvent molecule facilitates a water-mediated hydrogen bond between the side chain hydroxyl of Nrp2 T319, located at the base of the binding pocket, and the side chain guanidinium of VEGF-C R223 (Figure 2B). Likewise, a second solvent molecule bridges the side chain carboxylate of Nrp2 E351 and the free carboxylate of VEGF-C. These solvent-mediated interactions appear to further stabilize the position of the VEGF-C C terminus within the Nrp2-b1 binding pocket.

To confirm the critical role of the VEGF-C C terminus, we mutated the C-terminal arginine of VEGF-C to glutamate (R223E) and compared the ability of alkaline phosphatase (AP)-tagged VEGF-C and VEGF-C R223E to bind Nrp2-b1b2 affinity plates (Figure 2C). Robust binding was observed between AP-VEGF-C and Nrp2-b1b2, but R223E binding was reduced by >95%. These data demonstrate that the C-terminal arginine of mature VEGF-C is necessary for high-affinity Nrp2-b1b2 binding and confirm the importance of C-terminal propeptide processing within VEGF-C to produce a C-terminal arginine that allows avid engagement of Nrp2.

The interaction observed between Nrp2-b1 and VEGF-C buries 374 Å^2 surface area of the VEGF-C C terminus. This is comparable with that observed for the exon 8 encoded residues of VEGF-A (338 Å^2 buried surface area) (Figure 2D, dark gray) (Parker et al., 2012c) and tuftsin (328 Å^2 buried surface area) (Figure 2D, light gray) (Vander Kooi et al., 2007) which complex with an equivalent binding site on Nrp1-b1. Importantly, these ligands, like VEGF-C, also contain a C-terminal arginine. All three ligands traverse the L1 loop, an orientation that is maintained by the engagement of the carboxy terminus by the C-wall. Collectively, the shared use of a C-terminal arginine in VEGF-A and VEGF-C explains their ability to bind both Nrp receptors (Karpanen et al., 2006; Parker et al., 2012b), while electrostatic repulsion by the L1 loop and adjacent regions account for receptor selectivity (Figure 2D) (Parker et al., 2012b, 2012c).

Occluding the Nrp2 Interloop Cleft Abolishes Binding

The structure of VEGF-C in complex with Nrp2 reveals a critical role for the Nrp2-b1 interloop cleft, which forms the VEGF-C binding pocket. To confirm that the Nrp2 binding pocket is responsible for VEGF-C binding, we carried out site-directed mutagenesis of Nrp2-b1b2 to generate a construct with an occluded binding pocket. Specifically, T319, a residue at the base of the Nrp2-b1 interloop cleft, was mutated to arginine (Nrp2-T319R). We determined the crystal structure of Nrp2-T319R to a resolution of 2.4 Å (Figure 3A; Table 1). The R319 side chain showed clear electron density extending into the interloop cleft between the two binding pocket tyrosines, Y299 and Y356 (Figure 3B). Superimposing the VEGF-C/Nrp2 complex onto Nrp2-T319R demonstrates that the binding site occupied by VEGF-C is occluded in the Nrp2 mutant (Figure 3C). The Nrp2-T319R mutant was then used to analyze the contribution of the interloop cleft to VEGF-C binding. We compared the binding of VEGF-C with Nrp2-b1b2 and Nrp2-T319R (Figure 3D).

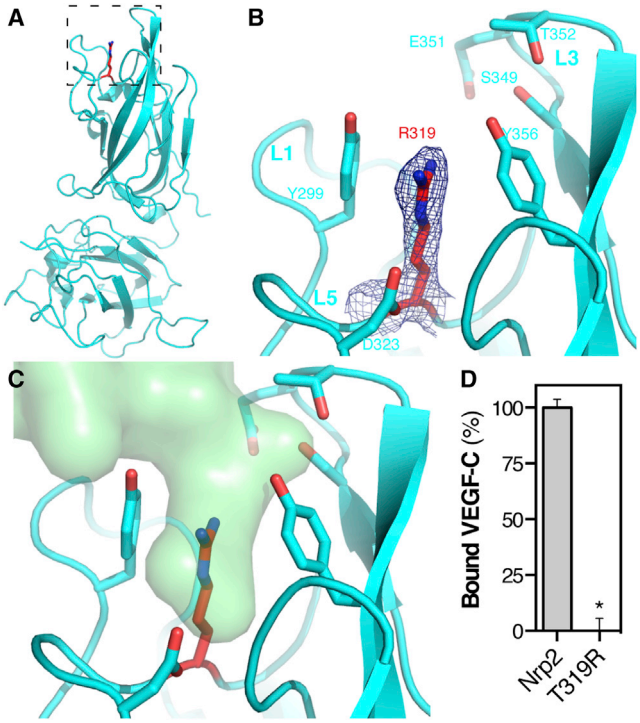

Figure 3. Crystal Structure and VEGF-C Binding Properties of Nrp2-T319R

(A) Structure of Nrp2-T319R with the stick representation for T319R shown in red.

(B) Zoom of the Nrp2-T319R binding pocket. The blue mesh illustrates the $2F_o - F_c$ electron density map for R319 contoured at 1.0σ.

(C) Superimposition of VEGF-C (green) onto the structure of Nrp2-T319R demonstrates that the binding pocket normally occupied by VEGF-C is blocked in the mutant.

(D) VEGF-C binding was compared between Nrp2-b1b2 and Nrp2-T319R. Binding was measured in triplicate and is reported as mean ± SD (*$p < 0.05$).

While robust binding was observed between AP-VEGF-C and Nrp2-b1b2, binding to Nrp2-T319R was completely abolished. These data confirm that the interloop cleft, formed by the Nrp2-b1 coagulation factor loops, forms a structure that uniquely accommodates the C terminus of VEGF-C to mediate binding of the C-terminally processed ligand.

A Dimeric Soluble Nrp2 Splice Form

Based on the specific binding of VEGF-C to the Nrp2 b1 domain, we hypothesized that the previously identified splice form of Nrp2, s_9Nrp2, could function as a selective inhibitor of VEGF-C. s_9Nrp2 is an alternative Nrp2 splice form that arises from intron inclusion in the b2 domain (Figure 4A). An in-frame stop codon encoded within the intron is predicted to result in termination of translation prior to the transmembrane domain, and thus production of a secreted Nrp2 receptor that contains the first two CUB domains (a1 and a2) and the first coagulation factor domain (b1), but only a portion of the coding sequence for the second coagulation factor domain (b2). Given that the b1 domain of Nrp2 is solely responsible for VEGF-C binding, we hypothesized that s_9Nrp2 may be able to effectively sequester VEGF-C, thereby functioning as an inhibitor. However, it is unknown whether the s_9Nrp2 transcript produces a functional protein, since s_9Nrp2 retains residues coding only a portion of the b2 domain (114 of 159 residues). Indeed, s_9Nrp2 lacks the coding region for three of the eight core β strands that normally integrate to form the distorted jelly-roll fold that typifies the b1 and b2 domains of Nrp. In addition, it was unknown whether s_9Nrp2 could accommodate the loss of the canonical C-terminal capping cysteine of the b2 domain. To investigate the physical and functional activity of s_9Nrp2, we tested the ability of this isoform to be secreted from eukaryotic cells. We produced s_9Nrp2 and a construct containing solely the ligand binding coagulation factor domains, s_9Nrp2^B (Figure 4A), as a human growth hormone (Hgh)-fusion in Chinese hamster ovary (CHO) cells. Western blot analysis demonstrated that both constructs were efficiently produced and secreted (Figure 4B). We next produced s_9Nrp2^B protein in bacteria. Analysis of s_9Nrp2^B by reducing SDS-PAGE revealed that purified s_9Nrp2^B, while running with a larger apparent molecular weight (MW) than Nrp2-b1 alone, was smaller than expected from its primary sequence (Figure 4C, observed MW = 22 kDa, expected MW = 34 kDa). Mass spectrometry confirmed that s_9Nrp2^B is an essentially homogeneous single species with MW = 22,775 Da ± 20 Da. These data, together with the observed intact N-terminal His-tag, indicate that s_9Nrp2^B is cleaved C-terminal to E457 (predicted MW = 22,792 Da). Thus, the proteolyzed s_9Nrp2^B contains only a single cysteine residue from the b2 domain (C434), which normally forms an intradomain disulfide. Surprisingly, under nonreducing conditions, s_9Nrp2^B ran with an apparent MW = 38 kDa, indicating the formation of a disulfide-linked intermolecular dimer via the free b2 domain cysteine (Figure 4C). Predominantly disulfide-linked dimeric protein is also observed in s_9Nrp2^B protein purified from CHO-cell conditioned media (Figure S3A). The difference in oligomeric state was evident from size exclusion chromatography (SEC) (Figure 4D). Nrp2-b1 eluted off SEC with an apparent MW = 16 kDa (gray line), while s_9Nrp2^B had an apparent MW = 38 kDa (black line), consistent with the SDS-PAGE analysis.

s_9Nrp2^B Is a Uniquely Potent Inhibitor of VEGF-C/Nrp2 Binding

To understand the structural arrangement of the s_9Nrp2^B dimer, we determined the crystal structure of s_9Nrp2^B to a resolution of 2.4 Å (Figure 5A; Table 1). Continuous electron density was observed from F275 to S453, consistent with the C terminus defined using mass spectrometry. A single dimer was present in the asymmetric unit, with the base of each b1 domain apposed to the other, thus forming an extended antiparallel dimer. The orientation of the dimer is stabilized by both the intermolecular disulfide and, unexpectedly, a unique dimeric helical bundle formed by residues from the b1-b2 linker and b2 domain (Figure 5B). The residues that form this unique helix (residues 428–453) display dramatic structural reorganization relative to that observed in the intact b2-domain, where they form an extended sheet and loop motif (Figure 5C). The C-terminal helix runs approximately 20° off parallel from the base of the b1 domain, an angle that is maintained by a cluster of hydrophobic residues at the hinge region between the helix and domain b1. The helix both caps the b1 domain and mediates the intermolecular interaction interface with the other monomer of the s_9Nrp2^B dimer.

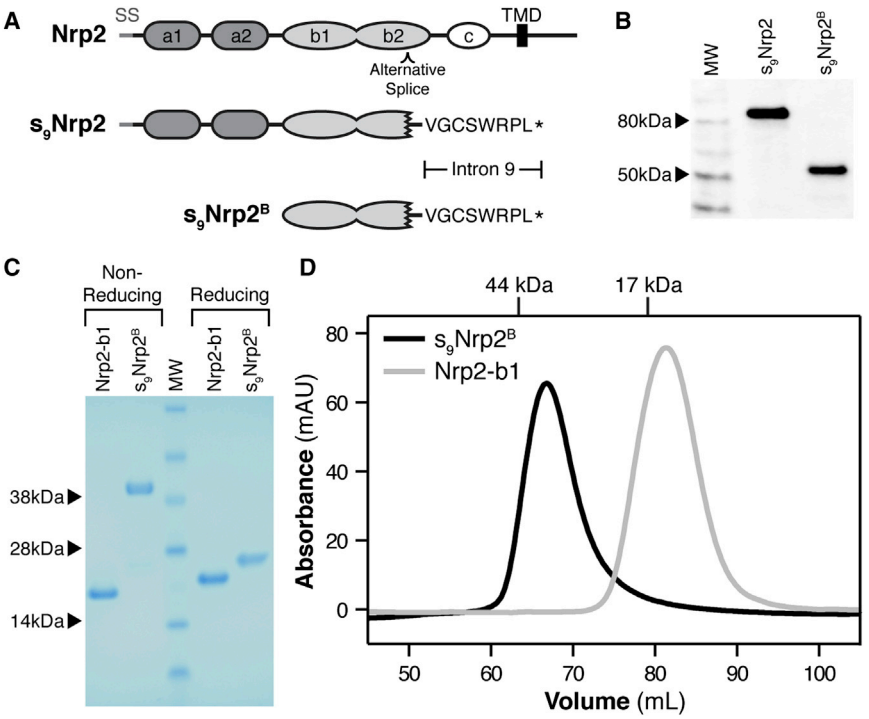

Figure 4. s_9Nrp2^B Forms a Disulfide-Linked Dimer

(A) Domain organization of Nrp2, s_9Nrp2, and the protein fragment used for our studies, s_9Nrp2^B. The intron 9-encoded sequence is indicated, which includes the in-frame stop codon (*).

(B) Western blot analysis of Hgh-tagged s_9Nrp2 and s_9Nrp2^B expressed in CHO cells.

(C) Nonreducing and reducing SDS-PAGE analysis of Nrp2-b1 and s_9Nrp2^B.

(D) The oligomeric state of s_9Nrp2^B (black line) was analyzed by size exclusion chromatography. Nrp2-b1 was run as a reference (gray line).

The intermolecular interface is composed of both helix-helix interactions, which are mostly hydrophobic in nature (Figure 5B), and helix-b1 interactions, which are mostly hydrophilic in nature. Truncation of the helix decreased the amount of dimeric species formed, demonstrating a role for the helix in the formation of a stable disulfide-linked dimer (Figure S3B).

The two binding pockets within the s_9Nrp2^B dimer are positioned 71 Å apart, suggesting that it could simultaneously engage both subunits of the VEGF-C dimer, which is 68 Å wide (Leppanen et al., 2010). Thus, we hypothesized that coengagement of both VEGF-C monomers by s_9Nrp2^B would allow the dimer to function as a uniquely potent inhibitor of VEGF-C/Nrp2 binding. To test this hypothesis, we compared the inhibitory potency of ATWLPPR, an optimized peptide inhibitor of Nrp that functions by competitive binding (Parker and Vander Kooi, 2014; Starzec et al., 2007), with Nrp2-b1 and s_9Nrp2^B, both of which function as soluble competitors through sequestration of VEGF-C (Figure 5D). ATWLPPR showed dose-dependent inhibition of VEGF-C binding to Nrp2 with an inhibitory concentration 50% (IC_{50}) = 10 μM (gray line), consistent with its modest reported potency. Next, we examined the ability of Nrp2-b1 to inhibit binding (blue line). Nrp2-b1 sequestered VEGF-C with improved potency compared with the peptide inhibitor, with an IC_{50} = 1.5 μM. As expected for a monomeric competitive inhibitor, the Hill slope was approximately –1 (ATWLPPR = –1.08 and Nrp2-b1 = –0.97). These data are consistent with independent engagement of each VEGF-C monomer by a single Nrp2-b1. Next, we measured the inhibitory potency of s_9Nrp2^B (orange line). Strikingly, s_9Nrp2^B potently sequestered VEGF-C with an IC_{50} = 250 nM, a significant improvement in potency from both the peptide inhibitor and Nrp2-b1. In addition, the Hill slope for s_9Nrp2^B was –1.5. Thus, the enhanced potency of s_9Nrp2^B is due to its ability to synergistically sequester the VEGF-C dimer through simultaneous and cooperative engagement of the two VEGF-C monomers.

VEGF-C signaling requires the coordinated action of Nrp2 and the RTK VEGFR3 (Xu et al., 2010). Nrp2 enhances signaling via VEGF-C through both a direct interaction with VEGF-C and via coupling with VEGFR3 (Favier et al., 2006). Thus, while s_9Nrp2^B could inhibit VEGF-C signaling by sequestering VEGF-C ligand from Nrp2, it is also possible that s_9Nrp2^B could interact with VEGFR3 and actually enhance VEGF-C binding and signaling. Therefore, we tested the effect of s_9Nrp2^B on VEGF-C binding to VEGFR3. While s_9Nrp2^B blocked VEGF-C binding to Nrp2, it showed no effect on VEGF-C binding to VEGFR3, indicating that the binding events are independent (Figure 5E).

We extended our studies to assess the efficacy of s_9Nrp2^B as an inhibitor of Nrp2 signaling in prostate cancer. Nrp2 and VEGF-C expression have both been reported to function in the survival and aggressiveness of prostate cancer (Goel et al., 2012; Muders et al., 2009). We assessed the ability of Nrp inhibition to reduce the formation of prostatospheres by C4-2 cells. Incubation with s_9Nrp2^B resulted in a significant decrease in prostatosphere formation (Figure 5F). Incubation with the specific Nrp inhibitor C-furSema (Goel et al., 2013; Parker et al., 2010) likewise significantly reduced prostatosphere formation, whereas the control C-Sema did not, demonstrating the specific role for Nrp in prostatosphere formation. These data demonstrate that s_9Nrp2^B can effectively sequester VEGF-C and raises the exciting possibility of using engineered Nrp ectodomains as inhibitors of pathological Nrp-dependent signaling (Figure 5G).

DISCUSSION

Structural characterization of the mechanism for VEGF-C binding to Nrp2 represents an important step for understanding the physiological and pathological activity of VEGF-C. These data also inform the rational design of specific VEGF-C/D antagonists, including s_9Nrp2^B, which potently inhibits VEGF-C/Nrp2 binding and represents a potential therapeutic avenue. Collectively, these results have important implications for interpreting both the aberrant loss and gain of function in the VEGF-C/Nrp2 signaling axis that critically underlies a number of disease states.

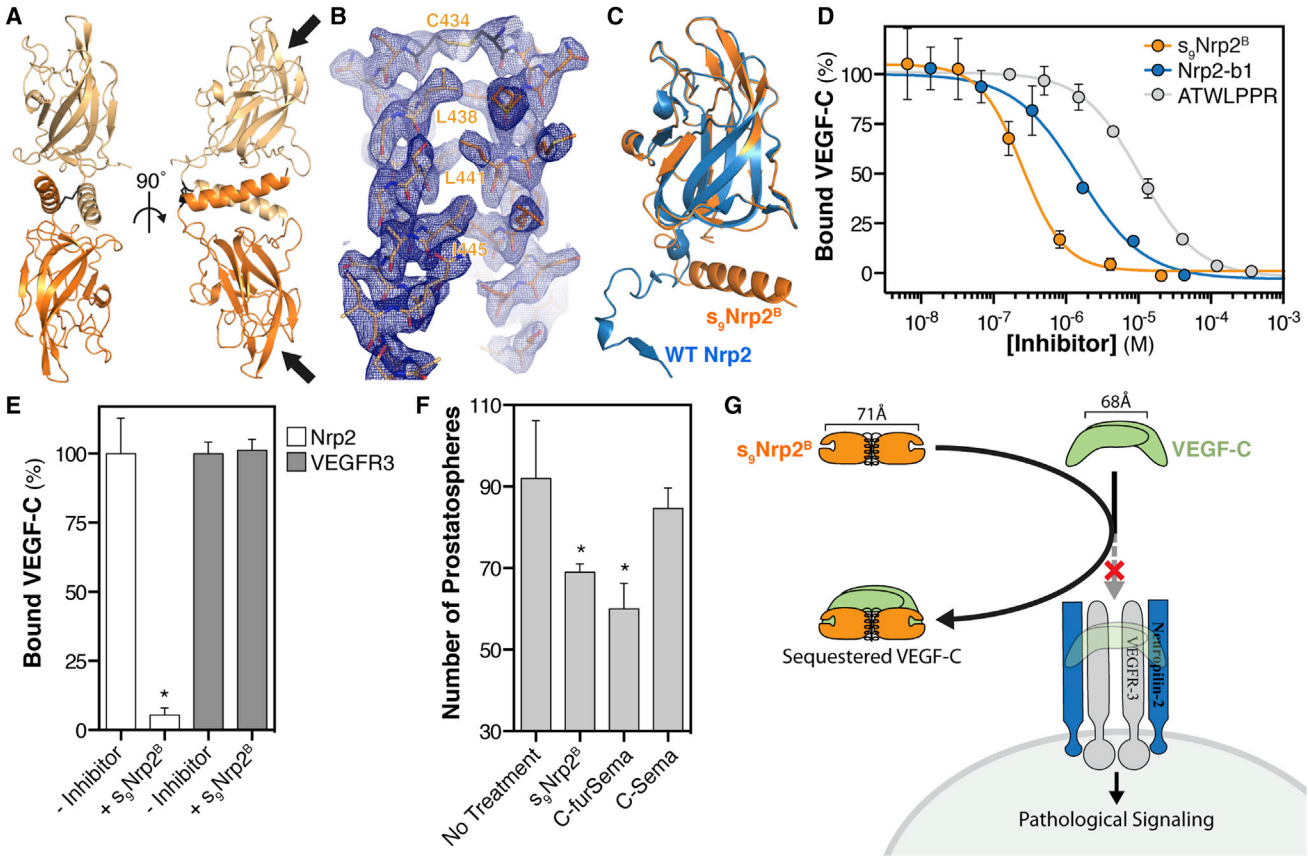

Figure 5. Crystal Structure and Inhibitory Properties of s_9Nrp2^B

(A) Crystal structure of the s_9Nrp2^B dimer (chain A, light orange; chain B, dark orange). The intermolecular disulfide is shown in black and the Nrp2-b1 binding pockets are labeled with arrows.

(B) Zoom of the dimeric helical bundle with the $2F_o - F_c$ electron density map contoured at 1σ.

(C) The residues of the Nrp2 b1-b2 linker and b2 domain show a dramatic structural reorganization from an extended loop in the b1b2 sequence (blue) to an extended helix in the s_9Nrp2^B dimer (orange).

(D) ATWLPPR (gray), Nrp2-b1 (blue), and s_9Nrp2^B (orange) were assayed for the ability to inhibit VEGF-C binding to Nrp2. ATWLPPR inhibited binding with an IC_{50} = 10 μM ($\log[IC_{50}] = -4.98 \pm 0.03$), Nrp2-b1 inhibited binding with an IC_{50} = 1.5 μM ($\log[IC_{50}] = -5.82 \pm 0.09$), and s_9Nrp2^B inhibited binding with an IC_{50} = 250 nM ($\log[IC_{50}] = -6.60 \pm 0.08$).

(E) s_9Nrp2^B was assayed for the ability to alter VEGF-C binding to VEGFR3. Addition of 4 μM s_9Nrp2^B fully inhibited VEGF-C/Nrp2 binding but showed no effect on VEGF-C/VEGFR3 binding.

(F) Inhibition of C4-2 cell prostatosphere formation was used to assess the biological activity of s_9Nrp2^B. Prostatosphere formation was compared in the absence and presence of s_9Nrp2^B, as well as with C-furSema (positive control) and C-Sema (negative control).

(G) Model illustrating the mechanism of action for s_9Nrp2^B. s_9Nrp2^B sequesters VEGF-C and prevents activation of the VEGFR3/Nrp2 signaling complex. All inhibition experiments were measured in triplicate and reported as mean ± SD (*$p < 0.05$).

With complementary biochemical and structural approaches, we show that VEGF-C C-terminal proteolysis is required for Nrp2 binding. The requirement for proteolytic processing is determined by the position of the Nrp2 C-wall, formed by the L3 coagulation factor loop residues, which specifically engages the VEGF-C free carboxy terminus, precluding binding of unprocessed protein. These results provide critical insight for interpreting the altered in vitro and in vivo functionality of alternative VEGF-C forms. While both N- and C-terminal processing regulate VEGF-C activity (Joukov et al., 1997; McColl et al., 2003), processing at these sites is not functionally equivalent. Indeed, loss of C-terminal processing is uniquely detrimental, fully ablating VEGF-C function in vivo (Khatib et al., 2010), which we demonstrate blocks Nrp2 binding.

The loss of VEGF-C binding to Nrp2-T319R, a mutant with an occluded binding pocket, demonstrates the use of a C-terminal arginine for ligand engagement. Indeed, the VEGF-C C-terminal arginine side chain and free carboxylate form extensive interactions with the Nrp2-b1 binding pocket. Interestingly, VEGF-C is not the only VEGF family member that, in the absence of post-translational modification, lacks a C-terminal arginine. Of the five VEGF family members, three contain Nrp binding domains that lack this structural motif (VEGF-C, VEGF-D, and VEGF-B_{186}). VEGF-D, a close structural and functional homolog of VEGF-C, is processed at an equivalent site in its C terminus to produce a C-terminal arginine (Stacker et al., 1999) and thus likely utilizes a similar binding mode to Nrp2. This observation provides additional functional insight, as loss of VEGF-D

C-terminal processing also ablates function in vivo (Harris et al., 2013). There are three VEGF-B isoforms, VEGF-B_{167}, VEGF-B_{127}, and VEGF-B_{186}, all of which differ in their C-terminal domain (Olofsson et al., 1996a, 1996b). Characterization of VEGF-B_{186} demonstrated that it exhibited proteolytic-dependent binding to Nrp1 and identified the site of proteolysis as R227 (Makinen et al., 1999). Thus, the mechanism of proteolytic-dependent VEGF-C binding to Nrp2 has broad explanatory power for understanding Nrp binding across the VEGF family.

Determining the structural basis for VEGF-C signaling via Nrp2 informs ongoing studies to describe the effect of signaling deficiency on human disease. Deficient VEGF-C signaling via Nrp2 has significant implications for both primary and secondary lymphedema. Mutations in both VEGFR-3 (Karkkainen et al., 2000) and VEGF-C (Gordon et al., 2013) have been demonstrated to underlie hereditary lymphedema and Nrp2 has been identified as an additional candidate gene (Ferrell et al., 2008; Karkkainen et al., 2001). In addition, both VEGF-C and Nrp2 have recently been identified as candidate genes for the development of secondary lymphedema following surgery in breast cancer (Miaskowski et al., 2013). The structural insights gleaned from the VEGF-C/Nrp2 complex also provide an important molecular basis for interpreting emerging exome sequencing data that has identified Nrp2 variants in close proximity to the ligand binding interface. Intriguingly, a stringent examination of exome sequencing data has reported both common and rare Nrp2 variants in human populations (Tennessen et al., 2012). Several of these variants are located in the coagulation factor loops of Nrp2-b1, the region to which VEGF-C binds. Specifically, there are two reported variants in the L5 loop (N321I and L322M), which are located proximal to the critical salt bridge formed by D323, and two in the L3 loop (Q353H and N354K). The structural data presented here provide a rationale for examining specific coagulation factor loop variants for loss of function on both a physical and functional level.

As opposed to aberrant VEGF-C loss of function in lymphedema, aberrant activation of VEGF-C signaling via Nrp2 is associated with cancer initiation, survival, and progression (Ellis, 2006; Stacker et al., 2002). The Nrp2/VEGF-C signaling axis contributes to tumorigenesis via multiple mechanisms. Mimicking its physiological function, VEGF-C signaling via Nrp2 stimulates lymphatic vessel recruitment to tumors and directly contributes to cancer metastasis (Caunt et al., 2008). Importantly, the role of VEGF-C and Nrp2 in tumorigenesis is not exclusively associated with aberrant lymphangiogenesis. Indeed, in situ studies have demonstrated that autocrine VEGF-C signaling in breast cancer cells stimulates cellular motility (Timoshenko et al., 2007). Further, recent reports indicate that cancer cell survival is enhanced through VEGF-C/Nrp2-dependent autophagy (Stanton et al., 2012) and that autocrine Nrp2 signaling maintains the population of cancer stem cells (Goel et al., 2013). VEGF-C also functions to protect prostate cancer cells from oxidative stress in an Nrp2-dependent fashion (Muders et al., 2009). Thus, selective inhibition of Nrp2 represents a promising, multipronged anticancer therapeutic strategy.

Secreted splice forms of angiogenic receptors have essential roles in vivo (Albuquerque et al., 2009; Ambati et al., 2006; Kendall and Thomas, 1993) and have been engineered to serve as therapeutic inhibitors that block aberrant pathway activation by ligand sequestration (Stewart, 2012). Here, we demonstrate that the alternative Nrp2 splice form, s_9Nrp2^B, potently sequesters VEGF-C and inhibits binding to Nrp2. The biological function and localized tissue-specific expression of s_9Nrp2 are of significant interest. Indeed, s_9Nrp2 may be analogous or complementary to sVEGFR-2, the secreted splice form of VEGFR-2 that functions as an endogenous lymphangiogenesis inhibitor (Albuquerque et al., 2009). VEGF-D also functions in lymphatic angiogenesis and has been shown to have partially overlapping biological function with VEGF-C and important pathological functions (Haiko et al., 2008; Harris et al., 2013; Karpanen et al., 2006). The conservation of Nrp2-interacting residues between VEGF-C and VEGF-D strongly suggests that s_9Nrp2^B will equivalently sequester both VEGF-C and VEGF-D. In contrast, the heparin-binding domain of VEGF-A contains specificity determinants that limit binding to Nrp2 (Parker et al., 2012b, 2012c). Thus, s_9Nrp2^B is likely to selectively sequester the lymphangiogenic-specific VEGF family members, VEGF-C and VEGF-D.

The practice of engineering inhibitor multimerization to increase potency is well established for soluble receptor fragments. Most commonly, soluble receptors are dimerized by expression as an Fc fusion protein (e.g., VEGF-trap). s_9Nrp2^B represents a unique mechanism for generation of a multimeric protein that maintains the benefits of avidity but does not require introduction of an exogenous polypeptide sequence. Additional optimization of s_9Nrp2^B potency, selectivity, and stability is an important future direction for the development of a therapeutically useful inhibitor.

EXPERIMENTAL PROCEDURES

Protein Expression and Purification

Human Nrp2-b1b2 (residues 276–595), human Nrp2-b1 (residues 276–430), human Nrp2-T319R (residues 276–595 with T319R mutation), s_9Nrp2^B (residues 275–555: isoform O60462-6), s_9Nrp2^B-Δ-helix (residues 276–436), and the Nrp2-b1b2/VEGF-C fusion were expressed in *E. coli* as His-tag fusion proteins from pET28b (Merck). Proteins were purified via immobilized metal ion affinity chromatography (IMAC) and either heparin affinity or SEC. AP-VEGF-C (residues 108–223) wild-type and mutant and Hgh-tagged proteins were produced by transient transfection of CHO cells (Aricescu et al., 2006). The VEGFR-3 extracellular domain was produced via baculovirus-mediated expression (residues 21–776) and purified by IMAC and SEC.

Structure Determination

Purified Nrp2-b1b2-VEGF-C fusion, Nrp2-T319R, and s_9Nrp2^B were concentrated to 2.0 mg/ml, 2.1 mg/ml, and 3.5 mg/ml, respectively, and crystals grown by hanging-drop vapor-diffusion experiments. Fusion protein crystals were obtained in 2 weeks at room temperature (RT) in 0.1 M MES (pH 6.5), 0.5 M ammonium sulfate. Nrp2-T319R crystals were obtained in 5 days at RT in 0.1 M HEPES (pH 7), 18% (w/v) PEG 12000. s_9Nrp2^B crystals were obtained in 2 weeks at RT in 10% PEG 1000/10% PEG 8000. Crystals were passed through mother liquor supplemented with 10% glycerol and then flash frozen in liquid nitrogen. Diffraction data were collected at the SER-CAT 22-ID and 22-BM beamlines of the Advanced Photon Source, Argonne National Laboratories and processed using HKL2000 (Otwinowski and Minor, 1997). Structures were solved by molecular replacement using Nrp2-b1b2 (PDB 2QQJ) followed by iterative modeling building and refinement using COOT (Emsley et al., 2010) and Refmac5 (Murshudov, 1997) to generate a final refined model (Table 1).

DSF

Peptides corresponding to processed and unprocessed VEGF-C were produced with an N-terminal tryptophan to allow accurate quantitation by UV_{280} absorbance (LifeTein LLC). Peptides were resuspended and combined with

2 μM of Nrp2-b1b2 and 5x SYPRO Orange Protein Gel Stain (Life Technologies) in PBS. Nrp2-b1b2 melting was monitored on a CFX96 Real-Time PCR system (Bio-Rad) from 20°C to 90°C at a rate of 1°C/50 s with fluorescent readings taken every 1°C.

Binding and Inhibition Assays

Plate binding and soluble Nrp competition assays were performed by measuring the binding of AP-tagged VEGF-C to Nrp2-b1b2, Nrp2-T319R, or VEGFR3 affinity plates. For direct binding assays, ligand was directly added to Nrp2-affinity plates, incubated for 1 hr at RT, washed, and developed using *p*-nitrophenyl phosphate AP substrate. For competition experiments, ligand was premixed with inhibitor and then added to affinity plates as with binding.

Prostatosphere Assays

Prostatosphere cultures used C4-2 prostate cancer cells (UroCor) (Cao et al., 2011). 5,000 cells/well were cultured in suspension in serum-free DMEM-F12 (Life Technologies), supplemented with B27 (1:50, Life Technologies), 20 ng/ml epidermal growth factor (Peprotech), and 4 μg/ml insulin (Sigma-Aldrich) in 6-well ultralow attachment plates (Corning). s_9Nrp2^B, C-furSema, or C-Sema inhibitors were added at a concentration of 5.0 μM while plating the cells. The prostatospheres were cultured for 6 days, and 1 ml of culture medium was added every other day. Spheres larger than 100 μm were counted.

ACCESSION NUMBERS

Coordinates and structure factors have been deposited in the PDB, www.pdb.org, with accession codes 4QDQ, 4QDR, 4QDS for the complex, T319R, and dimer structures, respectively.

SUPPLEMENTAL INFORMATION

Supplemental Information includes Supplemental Experimental Procedures and three figures and can be found with this article online at http://dx.doi.org/10.1016/j.str.2015.01.018.

ACKNOWLEDGMENTS

We thank Dr Carol Beach for assistance with mass spectrometry and Dr Hou-Fu Guo and Xiaobo Li for valuable advice and technical help. This work was supported by NIH Grants R01GM094155 (C.W.V.K), T32HL072743 (M.W.P.), DOD Prostate Cancer Grant PC111410 (A.M.M., H.L.G.), NIH P30GM103486 (Core support), and NSF REU DBI-1004931 (A.D.L.).

Received: May 14, 2014
Revised: January 15, 2015
Accepted: January 28, 2015
Published: March 5, 2015

REFERENCES

Adams, R.H., Lohrum, M., Klostermann, A., Betz, H., and Puschel, A.W. (1997). The chemorepulsive activity of secreted semaphorins is regulated by furin-dependent proteolytic processing. EMBO J. *16*, 6077–6086.

Albuquerque, R.J., Hayashi, T., Cho, W.G., Kleinman, M.E., Dridi, S., Takeda, A., Baffi, J.Z., Yamada, K., Kaneko, H., Green, M.G., et al. (2009). Alternatively spliced vascular endothelial growth factor receptor-2 is an essential endogenous inhibitor of lymphatic vessel growth. Nat. Med. *15*, 1023–1030.

Ambati, B.K., Nozaki, M., Singh, N., Takeda, A., Jani, P.D., Suthar, T., Albuquerque, R.J., Richter, E., Sakurai, E., Newcomb, M.T., et al. (2006). Corneal avascularity is due to soluble VEGF receptor-1. Nature *443*, 993–997.

Appleton, B.A., Wu, P., Maloney, J., Yin, J., Liang, W.C., Stawicki, S., Mortara, K., Bowman, K.K., Elliott, J.M., Desmarais, W., et al. (2007). Structural studies of neuropilin/antibody complexes provide insights into semaphorin and VEGF binding. EMBO J. *26*, 4902–4912.

Aricescu, A.R., Lu, W., and Jones, E.Y. (2006). A time- and cost-efficient system for high-level protein production in mammalian cells. Acta Crystallogr. D Biol. Crystallogr. *62*, 1243–1250.

Baldwin, M.E., Halford, M.M., Roufail, S., Williams, R.A., Hibbs, M.L., Grail, D., Kubo, H., Stacker, S.A., and Achen, M.G. (2005). Vascular endothelial growth factor D is dispensable for development of the lymphatic system. Mol. Cell. Biol. *25*, 2441–2449.

Cao, Q., Mani, R.S., Ateeq, B., Dhanasekaran, S.M., Asangani, I.A., Prensner, J.R., Kim, J.H., Brenner, J.C., Jing, X., Cao, X., et al. (2011). Coordinated regulation of polycomb group complexes through microRNAs in cancer. Cancer Cell *20*, 187–199.

Caunt, M., Mak, J., Liang, W.C., Stawicki, S., Pan, Q., Tong, R.K., Kowalski, J., Ho, C., Reslan, H.B., Ross, J., et al. (2008). Blocking neuropilin-2 function inhibits tumor cell metastasis. Cancer Cell *13*, 331–342.

Ellis, L.M. (2006). The role of neuropilins in cancer. Mol. Cancer Ther. *5*, 1099–1107.

Emsley, P., Lohkamp, B., Scott, W.G., and Cowtan, K. (2010). Features and development of Coot. Acta Crystallogr. D Biol. Crystallogr. *66*, 486–501.

Favier, B., Alam, A., Barron, P., Bonnin, J., Laboudie, P., Fons, P., Mandron, M., Herault, J.P., Neufeld, G., Savi, P., et al. (2006). Neuropilin-2 interacts with VEGFR-2 and VEGFR-3 and promotes human endothelial cell survival and migration. Blood *108*, 1243–1250.

Ferrell, R.E., Kimak, M.A., Lawrence, E.C., and Finegold, D.N. (2008). Candidate gene analysis in primary lymphedema. Lymphat. Res. Biol. *6*, 69–76.

Gagnon, M.L., Bielenberg, D.R., Gechtman, Z., Miao, H.Q., Takashima, S., Soker, S., and Klagsbrun, M. (2000). Identification of a natural soluble neuropilin-1 that binds vascular endothelial growth factor: in vivo expression and antitumor activity. Proc. Natl. Acad. Sci. USA *97*, 2573–2578.

Goel, H.L., Chang, C., Pursell, B., Leav, I., Lyle, S., Xi, H.S., Hsieh, C.C., Adisetiyo, H., Roy-Burman, P., Coleman, I.M., et al. (2012). VEGF/neuropilin-2 regulation of Bmi-1 and consequent repression of IGF-IR define a novel mechanism of aggressive prostate cancer. Cancer Discov. *2*, 906–921.

Goel, H.L., Pursell, B., Chang, C., Shaw, L.M., Mao, J., Simin, K., Kumar, P., Vander Kooi, C.W., Shultz, L.D., Greiner, D.L., et al. (2013). GLI1 regulates a novel neuropilin-2/alpha6beta1 integrin based autocrine pathway that contributes to breast cancer initiation. EMBO Mol. Med. *5*, 488–508.

Gordon, K., Schulte, D., Brice, G., Simpson, M.A., Roukens, M.G., van Impel, A., Connell, F., Kalidas, K., Jeffery, S., Mortimer, P.S., et al. (2013). Mutation in vascular endothelial growth factor-C, a ligand for vascular endothelial growth factor receptor-3, is associated with autosomal dominant milroy-like primary lymphedema. Circ. Res. *112*, 956–960.

Haiko, P., Makinen, T., Keskitalo, S., Taipale, J., Karkkainen, M.J., Baldwin, M.E., Stacker, S.A., Achen, M.G., and Alitalo, K. (2008). Deletion of vascular endothelial growth factor C (VEGF-C) and VEGF-D is not equivalent to VEGF receptor 3 deletion in mouse embryos. Mol. Cell. Biol. *28*, 4843–4850.

Harris, N.C., Davydova, N., Roufail, S., Paquet-Fifield, S., Paavonen, K., Karnezis, T., Zhang, Y.F., Sato, T., Rothacker, J., Nice, E.C., et al. (2013). The propeptides of VEGF-D determine heparin binding, receptor heterodimerization, and effects on tumor biology. J. Biol. Chem. *288*, 8176–8186.

He, Z., and Tessier-Lavigne, M. (1997). Neuropilin is a receptor for the axonal chemorepellent Semaphorin III. Cell *90*, 739–751.

Holash, J., Davis, S., Papadopoulos, N., Croll, S.D., Ho, L., Russell, M., Boland, P., Leidich, R., Hylton, D., Burova, E., et al. (2002). VEGF-Trap: a VEGF blocker with potent antitumor effects. Proc. Natl. Acad. Sci. USA *99*, 11393–11398.

Holmes, D.I., and Zachary, I. (2005). The vascular endothelial growth factor (VEGF) family: angiogenic factors in health and disease. Genome Biol. *6*, 209.

Janin, J. (1999). Wet and dry interfaces: the role of solvent in protein–protein and protein–DNA recognition. Structure *7*, R277–R279.

Jeltsch, M., Kaipainen, A., Joukov, V., Meng, X., Lakso, M., Rauvala, H., Swartz, M., Fukumura, D., Jain, R.K., and Alitalo, K. (1997). Hyperplasia of lymphatic vessels in VEGF-C transgenic mice. Science *276*, 1423–1425.

Joukov, V., Pajusola, K., Kaipainen, A., Chilov, D., Lahtinen, I., Kukk, E., Saksela, O., Kalkkinen, N., and Alitalo, K. (1996). A novel vascular endothelial growth factor, VEGF-C, is a ligand for the Flt4 (VEGFR-3) and KDR (VEGFR-2) receptor tyrosine kinases. EMBO J. *15*, 1751.

Joukov, V., Sorsa, T., Kumar, V., Jeltsch, M., Claesson-Welsh, L., Cao, Y., Saksela, O., Kalkkinen, N., and Alitalo, K. (1997). Proteolytic processing regulates receptor specificity and activity of VEGF-C. EMBO J. *16*, 3898–3911.

Karkkainen, M.J., Ferrell, R.E., Lawrence, E.C., Kimak, M.A., Levinson, K.L., McTigue, M.A., Alitalo, K., and Finegold, D.N. (2000). Missense mutations interfere with VEGFR-3 signalling in primary lymphoedema. Nat. Genet. *25*, 153–159.

Karkkainen, M.J., Saaristo, A., Jussila, L., Karila, K.A., Lawrence, E.C., Pajusola, K., Bueler, H., Eichmann, A., Kauppinen, R., Kettunen, M.I., et al. (2001). A model for gene therapy of human hereditary lymphedema. Proc. Natl. Acad. Sci. USA *98*, 12677–12682.

Karkkainen, M.J., Haiko, P., Sainio, K., Partanen, J., Taipale, J., Petrova, T.V., Jeltsch, M., Jackson, D.G., Talikka, M., Rauvala, H., et al. (2004). Vascular endothelial growth factor C is required for sprouting of the first lymphatic vessels from embryonic veins. Nat. Immunol. *5*, 74–80.

Karpanen, T., Heckman, C.A., Keskitalo, S., Jeltsch, M., Ollila, H., Neufeld, G., Tamagnone, L., and Alitalo, K. (2006). Functional interaction of VEGF-C and VEGF-D with neuropilin receptors. FASEB J. *20*, 1462–1472.

Karplus, P.A., and Faerman, C. (1994). Ordered water in macromolecular structure. Curr. Opin. Struct. Biol. *4*, 770–776.

Kendall, R.L., and Thomas, K.A. (1993). Inhibition of vascular endothelial cell growth factor activity by an endogenously encoded soluble receptor. Proc. Natl. Acad. Sci. USA *90*, 10705–10709.

Khatib, A.M., Lahlil, R., Scamuffa, N., Akimenko, M.A., Ernest, S., Lomri, A., Lalou, C., Seidah, N.G., Villoutreix, B.O., Calvo, F., et al. (2010). Zebrafish ProVEGF-C expression, proteolytic processing and inhibitory effect of unprocessed ProVEGF-C during fin regeneration. PLoS One *5*, e11438.

Kukk, E., Lymboussaki, A., Taira, S., Kaipainen, A., Jeltsch, M., Joukov, V., and Alitalo, K. (1996). VEGF-C receptor binding and pattern of expression with VEGFR-3 suggests a role in lymphatic vascular development. Development *122*, 3829–3837.

Leppanen, V.M., Prota, A.E., Jeltsch, M., Anisimov, A., Kalkkinen, N., Strandin, T., Lankinen, H., Goldman, A., Ballmer-Hofer, K., and Alitalo, K. (2010). Structural determinants of growth factor binding and specificity by VEGF receptor 2. Proc. Natl. Acad. Sci. USA *107*, 2425–2430.

Leppanen, V.M., Tvorogov, D., Kisko, K., Prota, A.E., Jeltsch, M., Anisimov, A., Markovic-Mueller, S., Stuttfeld, E., Goldie, K.N., Ballmer-Hofer, K., et al. (2013). Structural and mechanistic insights into VEGF receptor 3 ligand binding and activation. Proc. Natl. Acad. Sci. USA *110*, 12960–12965.

Lohela, M., Bry, M., Tammela, T., and Alitalo, K. (2009). VEGFs and receptors involved in angiogenesis versus lymphangiogenesis. Curr. Opin. Cell Biol. *21*, 154–165.

Lymboussaki, A., Olofsson, B., Eriksson, U., and Alitalo, K. (1999). Vascular endothelial growth factor (VEGF) and VEGF-C show overlapping binding sites in embryonic endothelia and distinct sites in differentiated adult endothelia. Circ. Res. *85*, 992–999.

Makinen, T., Olofsson, B., Karpanen, T., Hellman, U., Soker, S., Klagsbrun, M., Eriksson, U., and Alitalo, K. (1999). Differential binding of vascular endothelial growth factor B splice and proteolytic isoforms to neuropilin-1. J. Biol. Chem. *274*, 21217–21222.

McColl, B.K., Baldwin, M.E., Roufail, S., Freeman, C., Moritz, R.L., Simpson, R.J., Alitalo, K., Stacker, S.A., and Achen, M.G. (2003). Plasmin activates the lymphangiogenic growth factors VEGF-C and VEGF-D. J. Exp. Med. *198*, 863–868.

Miaskowski, C., Dodd, M., Paul, S.M., West, C., Hamolsky, D., Abrams, G., Cooper, B.A., Elboim, C., Neuhaus, J., Schmidt, B.L., et al. (2013). Lymphatic and angiogenic candidate genes predict the development of secondary lymphedema following breast cancer surgery. PLoS One *8*, e60164.

Muders, M.H., Zhang, H., Wang, E., Tindall, D.J., and Datta, K. (2009). Vascular endothelial growth factor-C protects prostate cancer cells from oxidative stress by the activation of mammalian target of rapamycin complex-2 and AKT-1. Cancer Res. *69*, 6042–6048.

Murshudov, G.N. (1997). Refinement of macromolecular structures by the maximum-likelihood method. Acta Crystallogr. D Biol. Crystallogr. *53*, 240–255.

Olofsson, B., Pajusola, K., Kaipainen, A., von Euler, G., Joukov, V., Saksela, O., Orpana, A., Pettersson, R.F., Alitalo, K., and Eriksson, U. (1996a). Vascular endothelial growth factor B, a novel growth factor for endothelial cells. Proc. Natl. Acad. Sci. USA *93*, 2576–2581.

Olofsson, B., Pajusola, K., von Euler, G., Chilov, D., Alitalo, K., and Eriksson, U. (1996b). Genomic organization of the mouse and human genes for vascular endothelial growth factor B (VEGF-B) and characterization of a second splice isoform. J. Biol. Chem. *271*, 19310–19317.

Otwinowski, Z., and Minor, W. (1997). Processing of X-ray diffraction data collected in oscillation mode. Macromol. Crystallogr. A *276*, 307–326.

Parker, M.W., and Vander Kooi, C.W. (2014). Microplate-based screening for small molecule inhibitors of neuropilin-2/vascular endothelial growth factor-C interactions. Anal. Biochem. *453*, 4–6.

Parker, M.W., Hellman, L.M., Xu, P., Fried, M.G., and Vander Kooi, C.W. (2010). Furin processing of semaphorin 3F determines its antiangiogenic activity by regulating direct binding and competition for neuropilin. Biochemistry *49*, 4068–4075.

Parker, M.W., Guo, H.F., Li, X., Linkugel, A.D., and Vander Kooi, C.W. (2012a). Function of members of the neuropilin family as essential pleiotropic cell surface receptors. Biochemistry *51*, 9437–9446.

Parker, M.W., Xu, P., Guo, H.F., and Vander Kooi, C.W. (2012b). Mechanism of selective VEGF-A binding by neuropilin-1-reveals a basis for specific ligand inhibition. PLoS One *7*, e49177.

Parker, M.W., Xu, P., Li, X., and Vander Kooi, C.W. (2012c). Structural basis for selective vascular endothelial growth factor-A (VEGF-A) binding to neuropilin-1. J. Biol. Chem. *287*, 11082–11089.

Parker, M.W., Linkugel, A.D., and Vander Kooi, C.W. (2013). Effect of C-terminal sequence on competitive semaphorin binding to neuropilin-1. J. Mol. Biol. *425*, 4405–4414.

Rose-John, S., and Heinrich, P.C. (1994). Soluble receptors for cytokines and growth factors: generation and biological function. Biochem. J. *300*, 281–290.

Rossignol, M., Gagnon, M.L., and Klagsbrun, M. (2000). Genomic organization of human neuropilin-1 and neuropilin-2 genes: identification and distribution of splice variants and soluble isoforms. Genomics *70*, 211–222.

Saaristo, A., Karkkainen, M.J., and Alitalo, K. (2002). Insights into the molecular pathogenesis and targeted treatment of lymphedema. Ann. N. Y. Acad. Sci. *979*, 94–110.

Siegfried, G., Basak, A., Cromlish, J.A., Benjannet, S., Marcinkiewicz, J., Chretien, M., Seidah, N.G., and Khatib, A.M. (2003). The secretory proprotein convertases furin, PC5, and PC7 activate VEGF-C to induce tumorigenesis. J. Clin. Invest. *111*, 1723–1732.

Soker, S., Fidder, H., Neufeld, G., and Klagsbrun, M. (1996). Characterization of novel vascular endothelial growth factor (VEGF) receptors on tumor cells that bind VEGF165 via its exon 7-encoded domain. J. Biol. Chem. *271*, 5761–5767.

Soker, S., Takashima, S., Miao, H.Q., Neufeld, G., and Klagsbrun, M. (1998). Neuropilin-1 is expressed by endothelial and tumor cells as an isoform-specific receptor for vascular endothelial growth factor. Cell *92*, 735–745.

Stacker, S.A., Stenvers, K., Caesar, C., Vitali, A., Domagala, T., Nice, E., Roufail, S., Simpson, R.J., Moritz, R., Karpanen, T., et al. (1999). Biosynthesis of vascular endothelial growth factor-D involves proteolytic processing which generates noncovalent homodimers. J. Biol. Chem. *274*, 32127–32136.

Stacker, S.A., Achen, M.G., Jussila, L., Baldwin, M.E., and Alitalo, K. (2002). Lymphangiogenesis and cancer metastasis. Nat. Rev. Cancer *2*, 573–583.

Stanton, M.J., Dutta, S., Zhang, H., Polavaram, N.S., Leontovich, A.A., Honscheid, P., Sinicrope, F.A., Tindall, D.J., Muders, M.H., and Datta, K. (2012). Autophagy control by VEGF-C/NRP-2 axis in cancer and its implication for treatment resistance. Cancer Res. *73*, 160–171.

Starzec, A., Ladam, P., Vassy, R., Badache, S., Bouchemal, N., Navaza, A., du Penhoat, C.H., and Perret, G.Y. (2007). Structure-function analysis of the

antiangiogenic ATWLPPR peptide inhibiting VEGF(165) binding to neuropilin-1 and molecular dynamics simulations of the ATWLPPR/neuropilin-1 complex. Peptides *28*, 2397–2402.

Stewart, M.W. (2012). Aflibercept (VEGF Trap-eye): the newest anti-VEGF drug. Br. J. Ophthalmol. *96*, 1157–1158.

Stuttfeld, E., and Ballmer-Hofer, K. (2009). Structure and function of VEGF receptors. IUBMB Life *61*, 915–922.

Tennessen, J.A., Bigham, A.W., O'Connor, T.D., Fu, W., Kenny, E.E., Gravel, S., McGee, S., Do, R., Liu, X., Jun, G., et al. (2012). Evolution and functional impact of rare coding variation from deep sequencing of human exomes. Science *337*, 64–69.

Timoshenko, A.V., Rastogi, S., and Lala, P.K. (2007). Migration-promoting role of VEGF-C and VEGF-C binding receptors in human breast cancer cells. Br. J. Cancer *97*, 1090–1098.

Vander Kooi, C.W., Jusino, M.A., Perman, B., Neau, D.B., Bellamy, H.D., and Leahy, D.J. (2007). Structural basis for ligand and heparin binding to neuropilin B domains. Proc. Natl. Acad. Sci. USA *104*, 6152–6157.

von Wronski, M.A., Raju, N., Pillai, R., Bogdan, N.J., Marinelli, E.R., Nanjappan, P., Ramalingam, K., Arunachalam, T., Eaton, S., Linder, K.E., et al. (2006). Tuftsin binds neuropilin-1 through a sequence similar to that encoded by exon 8 of vascular endothelial growth factor. J. Biol. Chem. *281*, 5702–5710.

Xu, Y., Yuan, L., Mak, J., Pardanaud, L., Caunt, M., Kasman, I., Larrivee, B., Del Toro, R., Suchting, S., Medvinsky, A., et al. (2010). Neuropilin-2 mediates VEGF-C-induced lymphatic sprouting together with VEGFR3. J. Cell Biol. *188*, 115–130.

Yuan, L., Moyon, D., Pardanaud, L., Breant, C., Karkkainen, M.J., Alitalo, K., and Eichmann, A. (2002). Abnormal lymphatic vessel development in neuropilin 2 mutant mice. Development *129*, 4797–4806.